Upright Light-Sheet Microscopy with Two-Photon Excitation for Imaging Large Samples

Takashi Saitou[1,2,*], Sota Takanezawa[3], Ryosuke Kawakami[4], Kana Kobayashi-Taguchi[5,6], Mai Kamito[4], Kana Takemoto[5,6], Yosuke Niko[7], Yuji Tsukamoto[1], Ryotaro Ozaki[1], Atsushi Tsurumune[3], Yoshiaki Kamei[5,6], Yuzo Umeda[6], Takeshi Imamura[2,4]

[1] Department of Electrical and Electronic Engineering, Graduate School of Science and Engineering, Ehime University, Ehime, Japan

[2] Translational Research Center, Ehime University Hospital, Ehime, Japan

[3] NIKON SOLUTIONS CO., LTD, Tokyo, Japan

[4] Department of Molecular Medicine for Pathogenesis, Graduate School of Medicine, Ehime University, Japan

[5] Department of Breast Center, Ehime University Hospital, Ehime, Japan

[6] Department of Hepato-Biliary-Pancreatic Surgery and Breast Surgery, Ehime University, Ehime, Japan

[7] Research and Education Faculty, Multidisciplinary Science Cluster, Interdisciplinary Science Unit, Kochi University, Kochi, Japan

Keywords: Fluorescence imaging, Light-sheet microscopy, Two-photon excitation, in vivo imaging, Optical clearing

Running title: Upright Two-Photon Light-sheet Microscopy

*Corresponding Author:

Takashi Saitou

Department of Electrical and Electronic Engineering, Graduate School of Science and Engineering, Ehime University, 3 Bunkyo-cho, Matsuyama, Ehime, 790-8577, Japan

E-mail: saito.takashi.qs@ehime-u.ac.jp

Tel.: +81 89 927 9765

Summary

Light-sheet microscopy has become a valuable tool for 3D imaging of biological samples, offering high resolution, fast imaging speeds, and minimal photodamage. Two-photon excitation further enhances its capabilities by providing deeper tissue penetration and reduced phototoxicity. However, conventional designs with orthogonal illumination and detection geometry often restrict the flexibility needed for imaging large or diverse samples that require varying immersion media. To address limitations in conventional systems for seamless imaging of both living organisms and cleared tissues, we developed an upright two-photon Bessel beam light-sheet microscope. Equipped with a middle-range magnification, multi-immersion objective lens (16x, NA 0.6), the microscope accommodates refractive indices ranging from 1.33 to 1.51. Built upon a previously established two-photon Bessel beam illumination system, this microscope maintains a large field of view while achieving cellular resolution. We demonstrated its versatility by applying it to both live specimen imaging and cleared tissue observation. For imaging optically cleared tissues, we implemented a method in which samples are immersed in a clearing agent and observed using coverslips. This enabled high-speed, large-scale imaging of human breast cancer tissues and mouse brain slices. The microscope's adaptability to different immersion media and its compatibility with coverslips offers significant flexibility for sample mounting, and this supports the imaging of large samples. By combining a laterally unconstrained configuration with two-photon excitation, this system advances the applicability of light-sheet microscopy across a wide range of biological research fields.

Introduction

Light-sheet microscopy has made significant advancements in recent years as a fluorescence microscopy technique capable of observing biomolecular and cellular functions in three dimensions with high speed and minimal photodamage to living organisms (Keller 2013, Power and Huisken 2017). In this microscopy, the detection and illumination optics are placed orthogonally, where a thin sheet of excitation light selectively illuminates the specimen at the focal plane of the detection objective lens. This configuration ensures that fluorescence emission originates from a single optical plane, enabling efficient excitation and detection, which achieves high-resolution, high-speed, and low-phototoxicity imaging.

Since the introduction of Selective Plane Illumination Microscopy (SPIM) (Huisken, Swoger et al. 2004), which utilizes cylindrical lenses to create selective optical planes, and Digital Scanning Light-Sheet Microscopy (DSLM) (Keller, Schmidt et al. 2008), which employs laser scanning techniques, numerous improvements have been reported to expand light-sheet microscopy technology. These include advanced beam engineering techniques such as multi-directional excitation (Huisken and Stainier 2007), multi-view imaging (Swoger, Verveer et al. 2007), and non-diffracting beams (Fahrbach, Simon et al. 2010, Planchon, Gao et al. 2011, Chen, Legant et al. 2014, Vettenburg, Dalgarno et al. 2014). Methodologies like two-photon excitation (Planchon, Gao et al. 2011, Truong, Supatto et al. 2011, Takanezawa, Saitou et al. 2021) and super-resolution imaging (Keller, Schmidt et al. 2010, Temma, Oketani et al. 2024) have further expanded its applications in life sciences. Furthermore, light-sheet microscopy is widely used for observing living multicellular organisms and also as a three-dimensional microscopy technique for optically cleared tissues. This application offers the advantages of

measuring large samples with high-speed imaging (Richardson and Lichtman 2015).

A key feature of light-sheet microscopy is its orthogonal geometry of the illumination and detection paths. Therefore, conventional systems typically place the objective lens and camera horizontally, a configuration adopted by many light-sheet microscopes. However, imaging optically cleared tissues often requires lateral imaging without constraints and continuous observation due to the large sample size. To address this, methods have been proposed where the objective lens is positioned above the sample, allowing imaging from above, as seen in ultramicroscopy (Dodt, Leischner et al. 2007) and CLARITY-optimized light-sheet microscopy (Tomer, Ye et al. 2014). Despite their advantages, these methods still face physical constraints in the arrangement of the objective lens and sample chamber, making them challenging to adapt for large or numerous samples and limiting their versatility and throughput.

To overcome these limitations, various microscope configurations have been developed, including upright, inverted, and single objective lens systems. Techniques such as inverted selective plane illumination microscopy (Wu, Ghitani et al. 2011), dual-view inverted selective-plane illumination microscopy (Wu, Wawrzusin et al. 2013, Kumar, Wu et al. 2014), light-sheet theta microscopy (Migliori, Datta et al. 2018), and open top light-sheet microscopy (McGorty, Liu et al. 2015, Strnad, Gunther et al. 2016, Glaser, Reder et al. 2017, Glaser, Reder et al. 2019) enable unconstrained lateral imaging, similar to conventional epi-fluorescence microscopy, and allow continuous observation without requiring sample repreparation. For example, dual-view inverted selective-plane illumination microscopy arranges the illumination and detection objective lenses at a 45° angle to the vertical axis, both immersed in an immersion medium. Open top light-sheet microscopy similarly

positions the lenses at a 45° angle but places them below the specimen. These designs eliminate lateral constraints while supporting high-resolution imaging of large samples.

Although these existing light-sheet microscopes accommodate samples with varying refractive indices while maintaining mid-range magnification and cellular resolution, two-photon excitation in light-sheet microscopy offers significant advantages for imaging living organisms and achieving improved penetration depth in partially cleared tissues. Previously, we developed a two-photon Bessel beam light-sheet microscope with a beam length of 600–1000 μm and a thickness of less than 5 μm, enabling long-term observation of whole live medaka fish development at cellular resolution (Takanezawa, Saitou et al. 2021). The use of a two-photon Bessel beam extends the propagation length while maintaining a narrow beam width, reducing the signal-to-noise ratio degradation caused by sidelobes. Combining a laterally unconstrained configuration with two-photon excitation further enhances the applicability of light-sheet microscopy. To fully exploit these advantages, we developed an upright light-sheet microscope equipped with a mid-range magnification, multi-immersion objective lens (16x, NA 0.6), capable of accommodating refractive indices ranging from 1.33 to 1.51. This microscope retains the orthogonal arrangement of the illumination and detection systems and employs horizontal scanning for continuous imaging over extended distances. Building upon our previously established two-photon Bessel beam illumination system, the new microscope achieves a large field of view while maintaining cellular resolution. We applied this microscope to both live specimen imaging and optically cleared tissue observation, demonstrating its adaptability to various immersion media. For optically cleared tissue imaging, we implemented a method in which samples are immersed in an optically clearing agent and observed using

coverslips with thiodiethanol (TDE) as the immersion medium. This approach successfully captured high-speed, large-scale images of cleared human breast cancer tissues and mouse brain slices, providing significant flexibility in sample mounting. The adaptability to different immersion media, along with its compatibility with coverslips, enables imaging of large or high-throughput samples, making this microscope highly adaptable for a wide range of applications.

Materials and Methods

Ethics statement

The animal experimental protocols were approved by the Committee on the Ethics of Animal Experiments of the Ehime University Graduate School of Medicine (approval number 05-RE-2-16) and conducted in accordance with the Guidelines for Animal Experiments of Ehime University and the Ethics Committee for Animal Experiments of Ehime University. Patient-derived samples were obtained from a patient diagnosed with estrogen receptor (ER)-positive invasive ductal carcinoma of the breast. A portion of the tumor was collected immediately after surgical excision and promptly stored at -80°C. This study was approved by the Institutional Review Board of the Ehime University School of Medicine (approval numbers 1807005 and 1701016). Written informed consent was obtained from the patient prior to sample collection.

Sample preparations

Medaka Fish Samples

Medaka fish were maintained in freshwater tanks with a water circulation system (LABREED, IWAKI) at 26–28 °C under a 14-hour light and 10-hour dark cycle (8:30–22:30 light). The fish were fed Artemia larvae and a powdered diet daily. Spawned eggs were collected in the morning and incubated in a dish containing diluted artificial seawater (0.03% w/v) with methylene blue. A transparent Medaka strain See-Through II (STII) (StrainID: MT112) (Wakamatsu, Pristyazhnyuk et al. 2001) was provided by the National BioResource Project (NBRP) Medaka (https://shigen.nig.ac.jp/medaka/). The transgenic FLT4-EGFP strain, which expresses EGFP

in lymphatic endothelial cells, was obtained from Dr. Deguchi (National Institute of Advanced Industrial Science and Technology) (Deguchi, Fujimori et al. 2012). All experiments were conducted in accordance with the guidelines of the safety committee for gene recombination experiments of Ehime University. Before microscopy observation, embryos were dechorionated using a hatching enzyme provided by NBRP Medaka. For imaging, embryo samples were embedded in 1% (w/v) agarose gel placed in a sample holder, which was positioned in a chamber filled with embryonic culture medium (ECM) (Kinoshita, Murata et al. 2009). For live imaging of lymphatic vessels, two FLT4-EGFP samples were used. For whole-body imaging of STII strain larvae, a pyrene-based push–pull dye, PC (HistoBright, Funakoshi), exhibiting fluorescence solvatochromism in response to lipids (Inoue, Kawakami et al. 2022) was used. Larvae were soaked in a 10 μM PC solution in ECM for 1 hour, followed by washing with ECM. For live imaging, two PC-stained larvae were used. Before microscopy observation, the embryos were embedded in 1% (w/v) agarose gel in ECM.

Mouse Samples

A male Thy1-YFP H transgenic mouse (Feng, Mellor et al. 2000), 10 weeks old, was used for experiments. The mouse was sacrificed by cervical dislocation, followed by cardiac perfusion with phosphate-buffered saline (PBS) to flush out blood before brain tissue collection. The brain was fixed by perfusion with 4% paraformaldehyde (PFA) in PBS for 12 minutes and then harvested. For sectioning, the brain tissue was embedded in 2% (w/v) agarose gel and sliced into 1 mm thick sections using a vibratome (VT1200, Leica). The sections were immersed in LUCID (ilLUminate Cleared organs to IDentify target molecules, PhotonTech Innovations) (Mizutani, Ono et al. 2018), an optical clearing agent composed of TDE, glycerol, and 40% non-

ionic organic iodine at a ratio of 50:5:45, for over two days. For light-sheet microscopy observation, the cleared sections were mounted on glass slides with LUCID solution, enclosed by a 1 mm width spacer (iSpacer 1.0mm, Sunjin Lab), and covered with a glass coverslip (C024321, Matsunami).

Human Breast Cancer Samples

Patient-derived breast cancer samples were fixed with 4% PFA for 24 hours at 4 °C. The samples then underwent an optical clearing process using the CUBIC (Clear, Unobstructed Brain/Body Imaging Cocktails and Computational analysis) method (Susaki, Tainaka et al. 2014). CUBIC-L and CUBIC-R reagents, as well as the CUBIC-HVTM1 3D immunostaining kit, were purchased from Tokyo Chemical Industry (T3740 for CUBIC-L, T3741 for CUBIC-R+(M), T3717 for CUBIC-HV1). Optical clearing and immunostaining procedures were performed according to the protocol provided by CUBICStars Inc. (Susaki, Shimizu et al. 2020). For delipidation, the samples were immersed in CUBIC-L for 2 days at room temperature. Nuclear staining was then performed using Hoechst 33342 diluted in HVTM I 3D Nuclear Staining Buffer, with the samples incubated for 3 days at room temperature. Subsequently, the samples were treated with a primary antibody, Anti-Estrogen Receptor alpha mAb (ab16660, Abcam), diluted in HVTM I 3D Immunostaining Buffer for 3 days at room temperature. Following this, secondary antibody staining was conducted using Alexa Fluor 488 anti-rabbit IgG (A11034, Invitrogen), also diluted in HVTM I 3D Immunostaining Buffer, for 3 days at room temperature. After thorough washing with PBS, the samples underwent post-fixation by immersion in 1% PFA at 4 °C for 24 hours, followed by an additional fixation step at 37 °C for 1 hour. After further washing with PBS, the buffer was replaced with CUBIC-R. For light-sheet microscopy observation, the samples were

mounted on glass slides with CUBIC-R solution, enclosed by a 1 mm width spacer (iSpacer 1.0 mm, Sunjin Lab), and covered with a glass coverslip (C024321, Matsunami).

Optical system

The upright light-sheet microscopy system was constructed based on a previous system (Takanezawa, Saitou et al. 2021, Saitou and Imamura 2023, Saitou and Imamura 2024), as illustrated in Figure 1A. For illumination, a femtosecond pulsed infrared laser (ALCOR 920-2, Spark Laser) was used, which emits pulses with a duration of <100 fs, a repetition rate of 80 MHz, and a wavelength of 920 nm. The power of the incident beam was modulated through a half-wave plate (HWP) and a Glan laser prism (GLP). The beam was then transmitted through a Bessel beam forming unit, where the incident Gaussian beam was expanded via a beam expander and passed through a lens-axicon triplet to create an annular ring pattern. As shown in Figure 1B, the tuned beam enters the illumination arm from the backside and exits at the front. This illumination arm consists of a galvano mirror scanner (Model 6200H, Cambridge Technology), a scan lens (SL50-2P2, Thorlabs), and a tube lens with a 200-mm focal length (TTL200-MP, Thorlabs). A 10× magnification water-dipping objective lens (CFI Plan Fluor 10× W, NA=0.3, Nikon) was used for illumination. The detection arm, positioned orthogonally to the illumination pathway, includes a 16× magnification multi-immersion lens (HC FLUOTAR L 16×, NA=0.6, Leica), a tube lens with a 200-mm focal length (TTL200-A, Thorlabs), and an sCMOS camera (Orca flash 4.0 v3, Hamamatsu Photonics) with a pixel size of 6.45 μm and a resolution of 2048×2048 pixels. These illumination and detection pathways are orthogonal to each other; they are positioned obliquely relative to the

optical table (Figure 1B). The light sheet was generated by scanning the beam along the *y*-direction using the galvano mirror scanner at a rate of 100 Hz. Images were recorded as unsigned 16-bit grayscale images. Along the emission pathway, a short-pass filter at 700 nm (Semrock) was inserted to block scattered excitation light. Additionally, bandpass filters at 465/30 nm, 520/35 nm, and 580/35 nm (center wavelength/bandwidth) (Semrock) were used for fluorescence detection. The sample chamber was mounted on an insert holder (MPRM, Thorlabs), which was attached to motorized stages (M403 and M-111, Physik Instrumente) controlling translation in the xyz-directions (Figure 1C). Image sequences were acquired by moving the motorized stages horizontally along the x-axis (Figure 1D). A custom software program written in LabVIEW 2015 (National Instruments) was used to control the camera, motorized stages, motorized filter wheel, and galvano mirror scanner.

Image processing

The measurement was performed by horizontal scanning along the *x*-axis, resulting in obliquely stacked image slices. To reconstruct images for accurate 3D representation, image processing using affine transformation was applied. This image reconstruction was performed using MATLAB software (MATLAB 2024a, MathWorks).

Evaluations of optical properties

To measure beam line profiles, the sample chamber was filled with a 10 μg/ml fluorescein solution. Beam extent and thickness were quantified by calculating FWHM (full width at half maximum) along the longitudinal and transverse axes. For evaluation of the microscopy resolution, 200-nm diameter yellow-green fluorescence beads (FluoSpheres, Thermo Fisher) embedded in 2% (w/v) agarose gel were imaged to determine PSFs (point spread functions). Following image reconstruction using affine transformation, PSFs were calculated by analyzing bead images using three-dimensional Gaussian fitting. All these calculations were performed using MATLAB software (MATLAB 2024a, MathWorks).

Statistical analysis

Beads PSF data are presented as box plots, where the boxes represent the first quantile, median, and third quantile. The upper and lower whiskers indicate the minimum and maximum values, respectively.

Results

Construction of up-right two-photon excitation light-sheet microscopy

We constructed an upright light-sheet microscopy system based on the two-photon excitation digital scanned light sheet microscope that we previously reported (Takanezawa, Saitou et al. 2021). The illumination system utilizes a Bessel beam, generated through a combination of an axicon and convex lenses, producing an extended beam profile (Figure 1A). The beam is transmitted to the illumination arm, which consists of a galvano scanner, a scan lens, and a tube lens. It enters from the back side and exits through the illumination objective (IO) at the front of the microscope. The illumination and detection arms are obliquely attached to a vertically positioned semi-circular breadboard and are placed orthogonally to each other (Figure 1B and C). For the upright configuration, we used a 10× water-dipping objective (CFI Plan Fluor 10× W, NA = 0.3, Nikon) for illumination and a 16× multi-immersion objective (HC FLUOTAR L 16×, NA = 0.6, Leica) for detection, making it possible to image various sample types, including optically cleared tissues. Stacked image sequences were acquired by moving motorized stages horizontally along the *x*-axis (Figure 1D), resulting in obliquely stacked slices that form a three-dimensional image. To reconstruct an accurate 3D representation, we applied an affine transformation method.

Performance of the upright light-sheet microscopy

To measure the beam line profiles, we used 10 μg/ml fluorescein solution dissolved in water, as well as optical clearing agents: 2,2'-thiodiethanol (TDE), CUBIC, and LUCID. For CUBIC and LUCID, considering their

application to tissue imaging, the fluorescein solutions were mounted on glass slides with a 1 mm height spacer and covered with a glass coverslip. TDE was used as the immersion medium for the objective lens (Figure 2). The refractive index of water is 1.33, whereas the refractive indices of the optical clearing reagents range from 1.49 (LUCID) to 1.51 (CUBIC and TDE). Therefore, adjustments to the beam profile were necessary to use the same system across different media. To achieve this, a convex lens with a 500 mm focal length was inserted before IO for water, while a concave lens with a −500 mm focal length was used for optical clearing reagents. To quantitatively compare these profiles, we extracted line profiles along the longitudinal and transverse directions at the beam waist (Figure 2A and B). The full width at half-maximum (FWHM) values were used to estimate beam length and thickness. The longitudinal beam extent was measured as 542.6 μm in water and 606 μm in TDE, while the transverse beam extent was 2.95 μm in water and 3.12 μm in TDE, indicating similar beam profiles between these two media. These data suggest that resolution can be maintained across media with different refractive indices. Next, we investigated the beam profiles for CUBIC and LUCID immersion media. The longitudinal beam extent was measured as 619.8 μm for CUBIC and 736.7 μm for LUCID, while the transverse beam extent increased to 9.35 μm in CUBIC and 11.35 μm in LUCID, indicating a reduction in axial resolution under these conditions (Figure 2C and D). These reductions result from the insertion of glass coverslips and refractive index mismatches, particularly in LUCID, which has a refractive index of 1.49.

To evaluate the microscope's resolution, we measured point spread functions (PSFs) using 500 nm diameter fluorescent beads (Figure 3A, B). To assess the positional variability of resolution along the beam axis, we divided the full-field images into three regions: center, right, and left (640 × 2048 pixels each), with the right

and left corresponding to the proximal and distal sides of beam injection, respectively. Three-dimensional Gaussian fitting was performed to estimate the beads' FWHM along the lateral and axial axes. We evaluated bead FWHM values for samples embedded in agarose in both water and CUBIC, as TDE and LUCID do not form a gel. The lateral resolution remained nearly unchanged between water and CUBIC. However, the axial resolution varied depending on beam thickness, with water providing better axial resolution than CUBIC across all three regions. This result is consistent with the beam profile measurements. Additionally, no significant differences were observed among the three regions, indicating that both axial and lateral resolutions were maintained across the field of view.

in vivo imaging application of light-sheet microscopy

To evaluate the performance of light-sheet microscopy for in vivo imaging, we conducted whole-body imaging of 1-week post-hatching (wph) larvae from the medaka FLT4-EGFP strain, which expresses EGFP in lymphatic endothelial cells and a part of venous vascular endothelial cells (Deguchi, Fujimori et al. 2012). Additionally, we imaged larvae of the See-Through II (STII) strain, stained with a pyrene-based push–pull dye (PC), which exhibits fluorescence solvatochromism in response to lipids. For imaging, the samples were embedded in 1% agarose within embryonic culture medium (ECM). Images were acquired with a 2 μm step size, a resolution of 1024 × 1024 pixels (0.8 μm × 0.8 μm per pixel), and an exposure time of 100 ms per slice, resulting in a single horizontal scan of more than 1800 slices, covering a total imaging depth of over 3600 μm. In the FLT4-EGFP strain, lymphatic vessels in the head, body trunk, and tail, as well as veins in the liver, were clearly visualized

(Figure 4A). In the STII strain, cellular silhouettes and capillary blood vessels were distinctly observed (Figure 4B). These results demonstrate that the microscope enables high signal-to-noise ratio and high resolution for in vivo imaging.

Optically cleared tissue imaging with light-sheet microscopy

To evaluate the performance of light-sheet microscopy for imaging optically cleared tissues, we performed imaging of human breast cancer samples and brain tissue from Thy1-YFP H-line transgenic mice. For breast cancer tissue, we applied the CUBIC-based optical clearing method following the protocol provided in the CUBIC-HVTM1 3D immunostaining kit. Using a primary antibody targeting the estrogen receptor (ER), images were acquired with a step size of 4 μm, a resolution of 1024 × 1024 pixels (0.81 μm × 0.81 μm/pixel), and an exposure time of 100 ms. A single horizontal scan consisting of 1316 slices was performed, covering a distance of approximately 5.2 mm. We captured two-channel color images using bandpass filters at 465/30 nm and 520/35 nm. The shorter wavelength bandpass corresponded to second harmonic generation (SHG) signals, while the longer wavelength bandpass detected Alexa Fluor 488 fluorescence from the secondary antibody against the estrogen receptor. To cover a larger imaging volume, three tiled stacks were acquired with ~15% overlap between each stack. After image stitching and applying an affine transformation, a combined 3D image was reconstructed, resulting in a final dataset of 20.8 GB with a resolution of 7998 × 2974 × 573 pixels per channel. The 3D image revealed the spatial distribution of fibrosis within the tumor stroma through SHG signals, alongside ER-positive breast cancer cells exhibiting proliferative characteristics while maintaining glandular

structures (Figure 5A, Supplemental Movie 1). A dense collagenous stroma is a characteristic feature of breast cancer, highlighting one of the key advantages of two-photon excitation.

Next, we imaged brain tissue from H-line transgenic mice expressing enhanced yellow fluorescent protein (EYFP) in a subset of neurons, enabling visualization of neural network structures. Images were acquired with a step size of 5 μm, a resolution of 1024 × 1024 pixels (0.81 μm × 0.81 μm/pixel), and an exposure time of 100 ms. A single horizontal scan consisting of more than 1800 slices was performed, covering a distance of over 9 mm. The fluorescence signals were detected using a bandpass filter at 520/35 nm. To capture a larger field of view, nine tiled image stacks were obtained with ~15% overlap. The entire imaging process took approximately 58.5 minutes. After stitching and applying an affine transformation, a combined 3D image of 97.6 GB with a resolution of 12,646 × 8,144 × 573 pixels was reconstructed. The 3D reconstruction enabled clear visualization of individual neurons and detailed neural network structures (Figure 5B, Supplemental Movie 2). Fluorescent signals from the axon bundles of the hippocampal commissure and anterior commissure were distinctly detected at depths of up to 500 μm from the tissue surface. Additionally, cortical layer V pyramidal neurons, including their somata and apical dendrites, were clearly observed.

Discussion

We developed an upright two-photon excitation light-sheet microscope utilizing a 16x, NA 0.6 middle-range magnification multi-immersion objective lens capable of adapting refractive indices ranging from 1.33 to 1.51. This microscope demonstrated its capability to observe a diverse range of samples, from living organisms to large optically cleared tissues, while maintaining cellular-level resolution. Furthermore, it is compatible with multi-well plates and coverslips, allowing for the imaging of large and high-throughput samples.

In this study, we implemented a method in which samples are immersed in a clearing agent and observed using coverslips with TDE as the immersion medium. This approach significantly improves the flexibility of sample mounting methods, enabling long-term preservation of stained samples and expanding its applications in biological imaging. However, there are some drawbacks to using coverslips. As shown in our results, issues such as decreased resolution and fluorescence intensity loss due to reflection at the coverslip interface arise. Although measuring fluorescence loss is difficult, in our case, sufficient performance was confirmed for both excitation light transmission and fluorescence signal detection. Nevertheless, depending on the arrangement of the illumination and detection optical axes, there may be a possibility that a high signal-to-noise ratio cannot be maintained.

For imaging human breast cancer tissue, we simultaneously captured SHG and fluorescence signals, allowing for the concurrent analysis of tumor markers and fibrous tissues. A defining characteristic of breast cancer is the development of a dense collagenous stroma, known as the desmoplastic reaction, which has been reported to correlate with the degree of fibrosis, tumor malignancy, and prognosis (Cardone, Tolino et al. 1997, Orimo,

Gupta et al. 2005, Kalluri and Zeisberg 2006). The desmoplastic reaction is driven by cancer cells activating surrounding fibroblasts and cancer-associated fibroblasts (CAFs), resulting in excessive production of the extracellular matrix (Orimo, Gupta et al. 2005). In the examined breast cancer sample, the three-dimensional distribution of fibrosis within the tumor stroma was clearly visualized using SHG, alongside ER-positive breast cancer cells that exhibited proliferation while maintaining glandular structures (Figure 5A). The extracellular matrix is also recognized as a key factor contributing to therapeutic resistance in various solid tumors (Prakash and Shaked 2024). Therefore, SHG, which provides label-free visualization of stromal fibrosis as a component of the extracellular matrix, is a valuable tool for studying the tumor microenvironment. Furthermore, by applying fluorescent staining to the optically cleared breast cancer tissue and imaging it with this advanced light-sheet microscope, we could comprehensively evaluate the spatial relationships between fibrosis and cancer cells within the tumor microenvironment. This integrated approach may offer insights into predicting treatment resistance and determining the prognosis of breast cancer.

A significant benefit of two-photon excitation is reduced photobleaching, allowing for prolonged and repeated observations. Additionally, it improves deep tissue penetration, making it suitable for samples that are not completely transparent or are relatively thick. Given these advantages, this method is expected to be applicable to other tissues, such as liver, bone, and cartilage (Saitou, Kiyomatsu et al. 2018), beyond breast cancer tissue. Furthermore, it holds potential for contributing to the advancement of digital pathology in combination with computational image processing technology (Saitou, Kiyomatsu et al. 2018, Saitou, Takanezawa et al. 2018, Kobayashi-Taguchi, Saitou et al. 2022).

In upright and inverted configurations, the oblique placement of the objective lens reduces the effectively usable working distance and limits imaging depth. This contrasts with conventional setups, where the full working distance of DO lens can be utilized. For example, the objective lenses used in this study have working distances of 2.5 mm (DO) and 3.5 mm (IO), but due to their placement at angles of approximately 30° and 120° from the vertical, respectively, the imaging depth is limited to about 1 mm due to geometric constraints. To extend imaging depth, lenses with longer working distances could be used, or the objective lens angle could be adjusted closer to the vertical. However, the latter requires constructing an angled optical system, such as light-sheet theta microscopy, which reduces the field of view. To address this issue, the development of long-working distance objective lenses and detection optical systems compatible with oblique illumination may be necessary. Upright configurations offer the advantage of easy objective lens exchange and no need for specialized holders. In contrast, inverted configurations allow for a wider range of applications due to compatibility with commercially available glass-bottom multi-well plates. Single-objective-lens systems (Dunsby 2008) have drawbacks such as a limited field of view and reduced resolution when using low-NA objective lenses, but they effectively utilize the objective lens's working distance. Thus, selecting the appropriate microscope configuration requires careful consideration of factors such as working distance, imaging depth, and sample types.

Acknowledgments

We would like to express sincere grateful to “National BioResource Project (NBRP) Medaka” for providing the hatching enzyme. This work was supported by the MEXT/JSPS KAKENHI Grant Number JP24K15178, the JST FOREST Program (Grant Number JPMJFR226R), the Nakatani Foundation for Advancement of Measuring Technologies in Biomedical Engineering, and the Research Foundation for Opto-Science and Technology, and the Uehara Memorial Foundation to T.S. Additionally, this work is supported by the MEXT/JSPS KAKENHI Grant Number JP24K02567, and JP16H06280 “Advanced Bioimaging Support” to T.I.. TI was also supported by the Naito Foundation, the Uehara Memorial Foundation, and the Research Grant of the Princess Takamatsu Cancer Research Fund (23-255005).

Competing interests

S.T. and A.T. are employees of NIKON SOLUTIONS CO., LTD. The remaining authors declare that they have no competing interests.

Figures

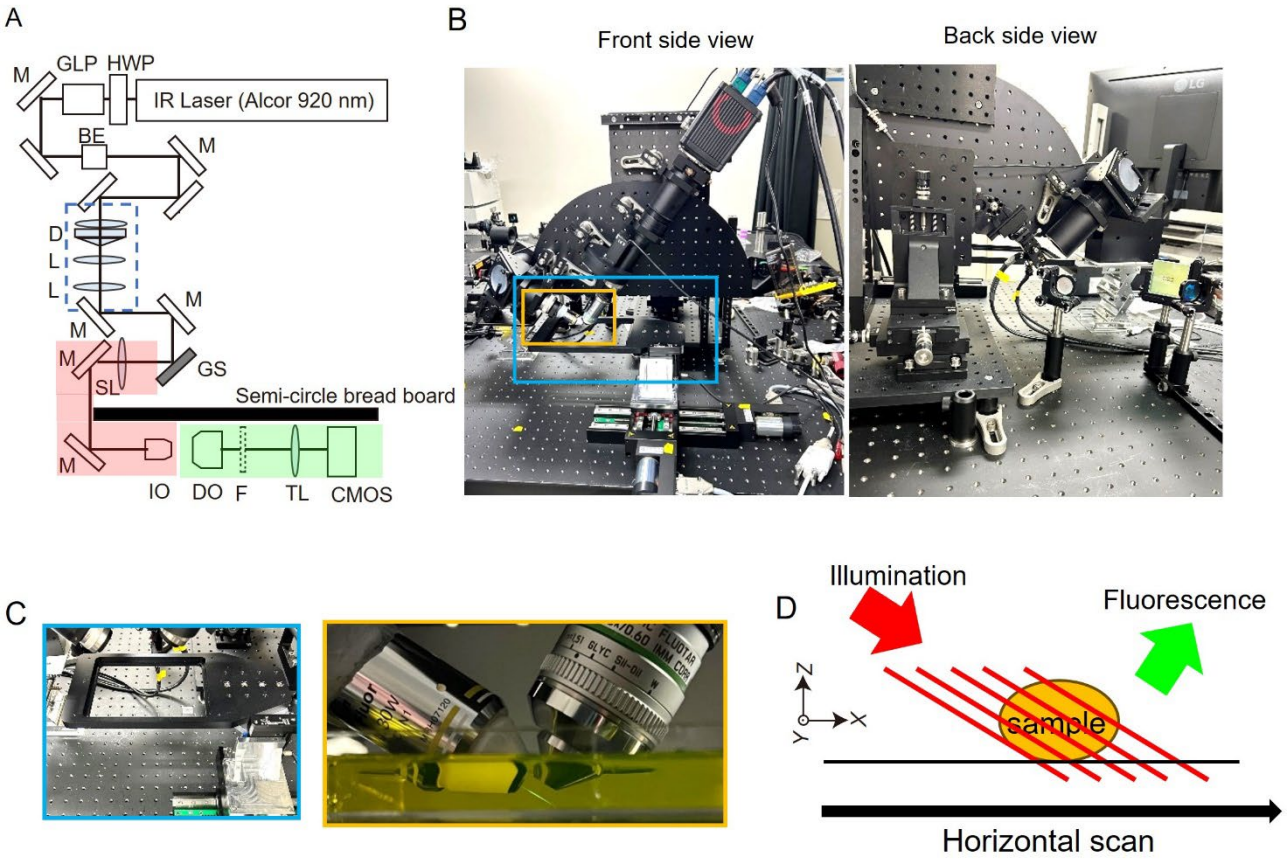

Figure 1. Microscope system. (A) Optical scheme of the upright two-photon Bessel beam excitation light-sheet microscopy. For illumination, a femtosecond pulsed laser system, ALCOR 920-2 (920 nm wavelength) was used as the laser source. The Bessel beam formation unit indicated by the dashed blue rectangle was incorporated into the system. A galvano mirror scanner, a scan lens, and a tube lens were used to generate the light-sheet. The resulting optical slice was imaged through DO lens, a tube lens, and an sCMOS camera, with the illumination and detection pathways set perpendicularly to each other. (B) Front and back side views of the microscope. The generated Bessel beam was transmitted through the illumination arm from the back side and exited at the front. This arm contains the galvo mirror scanner, a scan lens, a tube lens, and IO lens, which is a 10× magnification water-dipping objective (CFI Plan Fluor 10× W, NA=0.3, Nikon). (C) Magnified views of the sample holder

and objective lenses. The sample holder and objective lenses, highlighted by blue and orange rectangles in (B), respectively, are shown in detail. The sample holder was controlled by motorized xyz stages. The illumination and detection pathways were positioned orthogonally. To enable the use of various immersion media, including water and optical clearing reagents with high refractive indices, a multi-immersion objective lens (HC FLUOTAR L 16×, NA = 0.6, Leica) was used. (D) Scanning mode of image acquisition. Stacked image sequences were acquired by translating the motorized stages horizontally along the x-axis. Abbreviations; HWP, half-wave plate; GLP, Glan-laser prism; M, mirror; BE, beam expander; D axicon lens doublet; GM, galvano mirror scanner; SK, scan lens; TL, tube lens; F, emission filter.

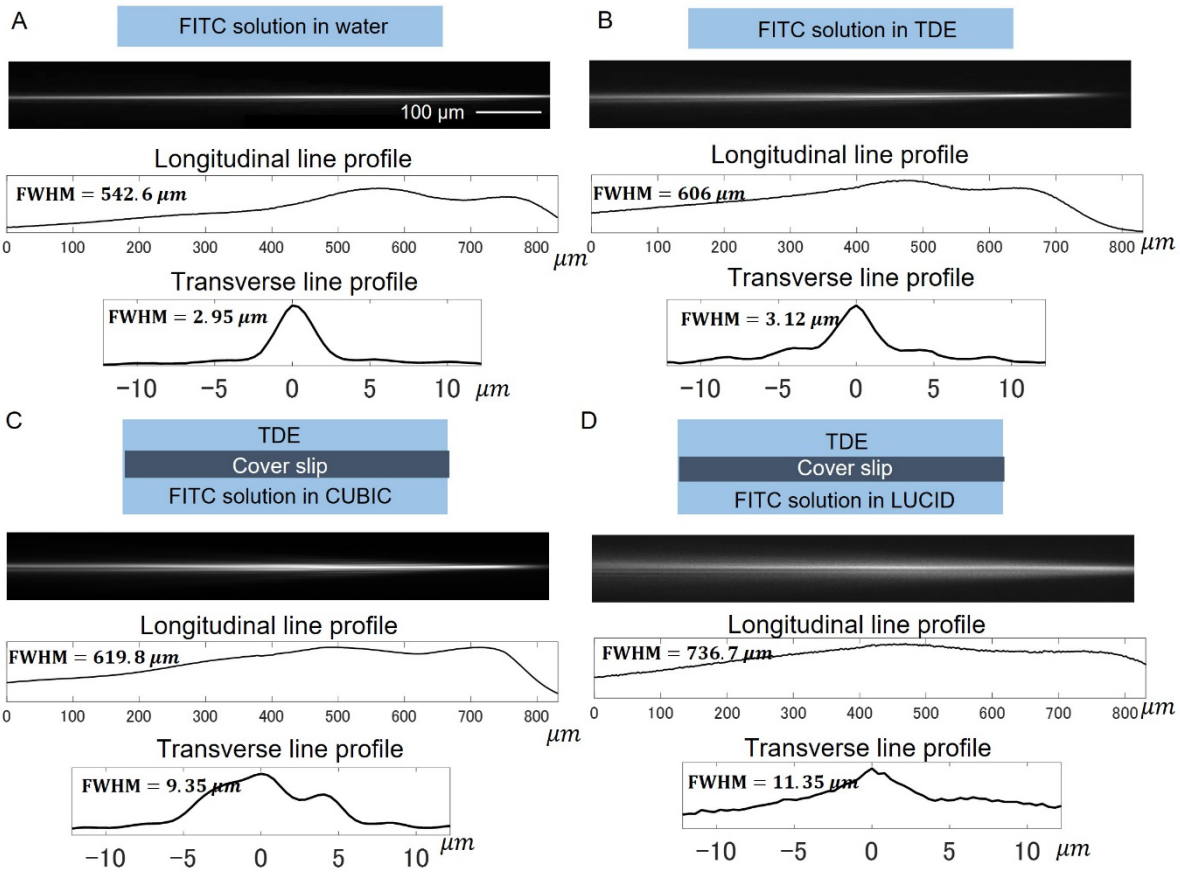

Figure 2. Comparisons of beam line profiles under different immersion medium conditions. The beam line profiles were measured based on fluorescent signals emitted by a fluorescein solution (10 μg/mL). Intensity profiles along both the longitudinal and transverse directions, as well as FWHM (full width at half maximum) values for signal extents, were evaluated. (A) Fluorescein dissolved in water, with lenses immersed directly in the solution. (B) Fluorescein dissolved in TDE, with lenses immersed directly in the solution. (C) Fluorescein dissolved in the CUBIC agent, covered with a glass coverslip (thickness: 0.13–0.17 mm), with lenses immersed in TDE applied on top of the coverslip. (D) Fluorescein dissolved in the LUCID agent, covered with a glass coverslip (thickness: 0.13–0.17 mm), with lenses immersed in TDE applied on top of the coverslip.

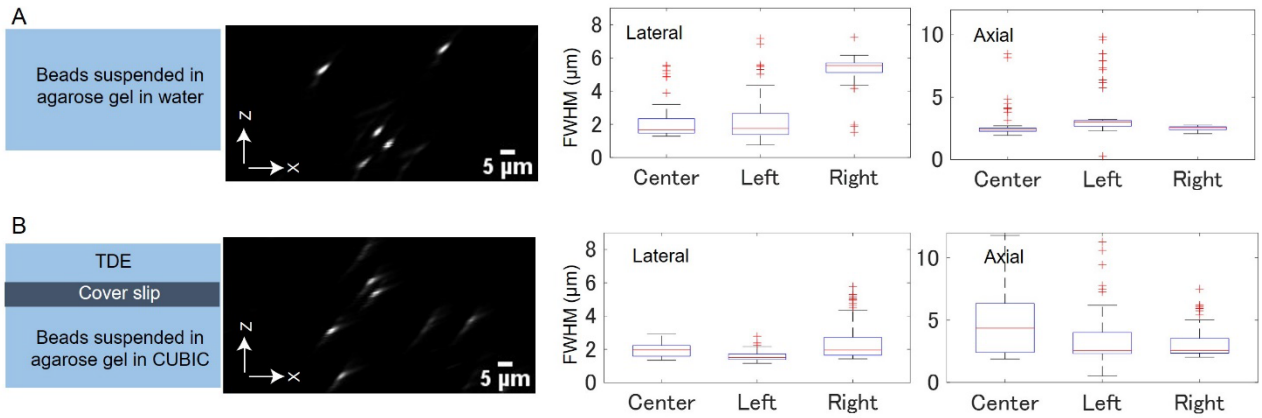

Figure 3. Measurement of lateral and axial PSFs for different medium conditions: water (A) and CUBIC (B). Fluorescent beads were embedded in 2% (w/v) agarose gel prepared in either water or CUBIC, and images were acquired using the respective setups. For visualization, maximum intensity projections along the *y*-axis were performed. The PSFs were quantified using FWHM values in the lateral and axial directions. These calculations employed independent beads as data points: Water (center n=89, left n=57, right n=40), CUBIC (center n=176, left n=100, right n=105). In the box plots, the boxes represent the first quantile, median, and third quantile. Lower and upper whiskers indicate the minimum and maximum values, respectively, excluding outliers. The red line represents the mean value.

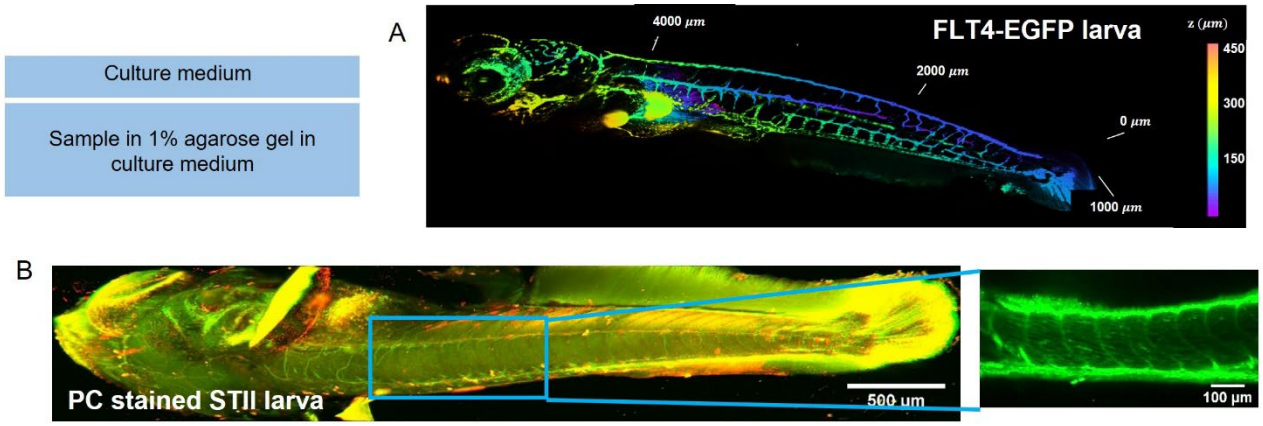

Figure 4. Application to in vivo imaging of medaka larvae. The samples were embedded in 1% (w/v) agarose dissolved in embryonic culture medium, which was also used as the immersion medium. (A) Whole-body imaging of a FLT4-EGFP transgenic larva (1 wph). The image was acquired using a bandpass filter (520/35 nm) and visualized using a volume rendering method, where different colors represent different *z*-positions. (B) Whole-body imaging of an STII strain larva stained with PC. The image was acquired using bandpass filters at 520/35 nm (green) and 580/35 nm (red). A merged image was generated using maximum intensity projection along the *z*-axis. A magnified image was extracted from the green channel of the whole-body image.

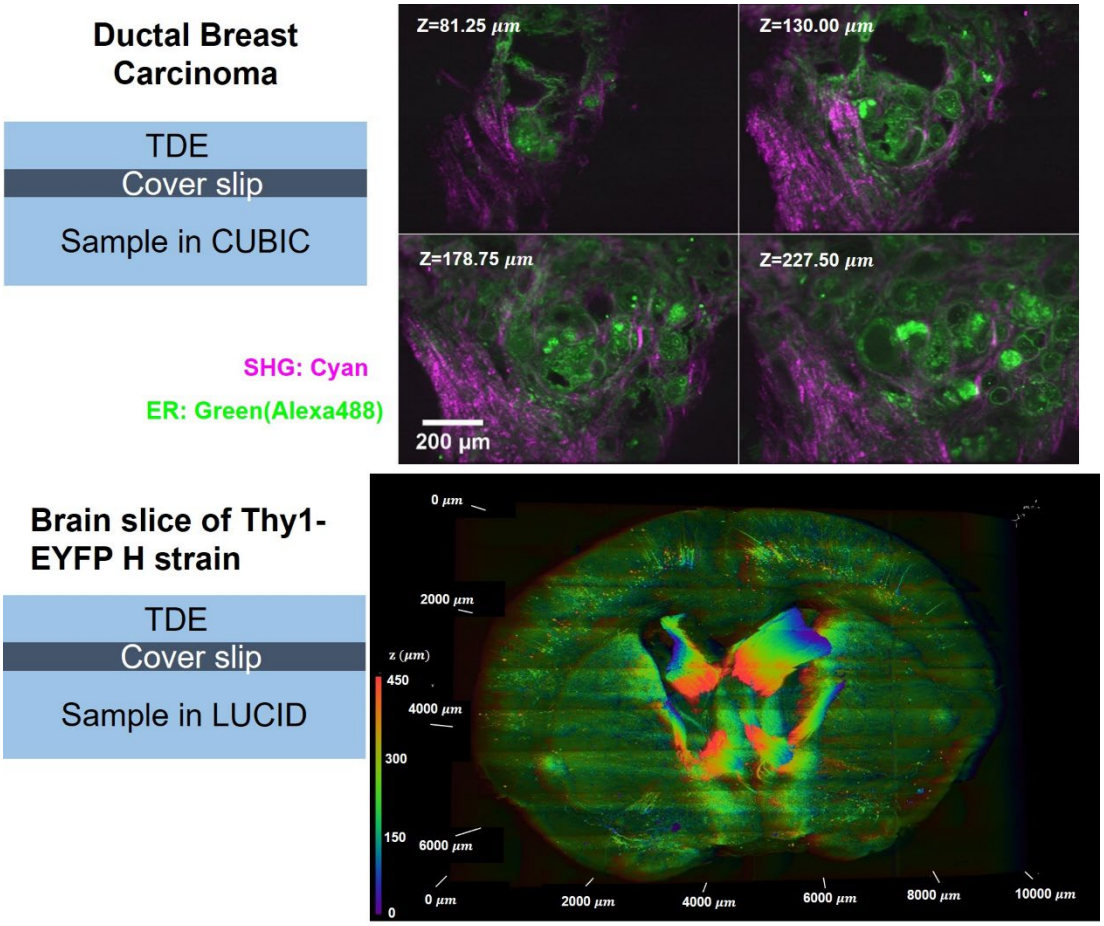

Figure 5. Application to optically cleared tissue imaging. (A) Two-channel images of a CUBIC-based optically cleared ER-positive invasive ductal carcinoma of the breast. The sample was cleared using the CUBIC method and histologically stained with an estrogen receptor (ER) antibody following the CUBIC-HistoVision protocol described in the Materials and Methods section. The magenta-colored image represents the SHG signal. The green and magenta images were acquired using bandpass filters at 520/35 nm and 465/30 nm, respectively. White values indicate the z-position from the top surface of the tissue. The sample was mounted in CUBIC reagent, covered with a glass coverslip, and immersed in TDE for imaging. (B) Brain slice image from a ten-week-old male Thy1-YFP H transgenic mouse. The left panel shows color-coded images representing different z-positions, while the right panel displays images from individual z-slices. The sample was optically cleared

using the LUCID method. For mounting, the sample was immersed in LUCID reagent, covered with a glass coverslip, and further immersed in TDE.

References

Cardone, A., A. Tolino, R. Zarcone and E. Tartaglia (1997). "Prognostic value of desmoplastic reaction and lymphocytic infiltration in the management of breast cancer." Panminerva medica **39**(3): 174-177.

Chen, B. C., W. R. Legant, K. Wang, L. Shao, D. E. Milkie, M. W. Davidson, C. Janetopoulos, X. S. Wu, J. A. Hammer, 3rd, Z. Liu, B. P. English, Y. Mimori-Kiyosue, D. P. Romero, A. T. Ritter, J. Lippincott-Schwartz, L. Fritz-Laylin, R. D. Mullins, D. M. Mitchell, J. N. Bembenek, A. C. Reymann, R. Bohme, S. W. Grill, J. T. Wang, G. Seydoux, U. S. Tulu, D. P. Kiehart and E. Betzig (2014). "Lattice light-sheet microscopy: imaging molecules to embryos at high spatiotemporal resolution." Science **346**(6208): 1257998.

Deguchi, T., K. E. Fujimori, T. Kawasaki, K. Maruyama and S. Yuba (2012). "In vivo visualization of the lymphatic vessels in pFLT4-EGFP transgenic medaka." Genesis **50**(8): 625-634.

Dodt, H.-U., U. Leischner, A. Schierloh, N. Jährling, C. P. Mauch, K. Deininger, J. M. Deussing, M. Eder, W. Zieglgänsberger and K. Becker (2007). "Ultramicroscopy: three-dimensional visualization of neuronal networks in the whole mouse brain." Nature methods **4**(4): 331-336.

Dunsby, C. (2008). "Optically sectioned imaging by oblique plane microscopy." Optics express **16**(25): 20306-20316.

Fahrbach, F. O., P. Simon and A. Rohrbach (2010). "Microscopy with self-reconstructing beams." Nature Photonics **4**(11): 780.

Feng, G., R. H. Mellor, M. Bernstein, C. Keller-Peck, Q. T. Nguyen, M. Wallace, J. M. Nerbonne, J.

W. Lichtman and J. R. Sanes (2000). "Imaging neuronal subsets in transgenic mice expressing multiple spectral variants of GFP." Neuron **28**(1): 41-51.

Glaser, A. K., N. P. Reder, Y. Chen, E. F. McCarty, C. Yin, L. Wei, Y. Wang, L. D. True and J. T. Liu (2017). "Light-sheet microscopy for slide-free non-destructive pathology of large clinical specimens." Nature biomedical engineering **1**(7): 0084.

Glaser, A. K., N. P. Reder, Y. Chen, C. Yin, L. Wei, S. Kang, L. A. Barner, W. Xie, E. F. McCarty and C. Mao (2019). "Multi-immersion open-top light-sheet microscope for high-throughput imaging of cleared tissues." Nature communications **10**(1): 2781.

Huisken, J. and D. Y. Stainier (2007). "Even fluorescence excitation by multidirectional selective plane illumination microscopy (mSPIM)." Opt Lett **32**(17): 2608-2610.

Huisken, J., J. Swoger, F. Del Bene, J. Wittbrodt and E. H. Stelzer (2004). "Optical sectioning deep inside live embryos by selective plane illumination microscopy." Science **305**(5686): 1007-1009.

Inoue, K., R. Kawakami, M. Murakami, T. Nakayama, S. Yamamoto, K. Inoue, T. Tsuda, K. Sayama, T. Imamura and D. Kaneno (2022). "Synthesis and photophysical properties of a new push–pull pyrene dye with green-to-far-red emission and its application to human cellular and skin tissue imaging." Journal of Materials Chemistry B **10**(10): 1641-1649.

Kalluri, R. and M. Zeisberg (2006). "Fibroblasts in cancer." Nature reviews cancer **6**(5): 392-401.

Keller, P. J. (2013). "Imaging morphogenesis: technological advances and biological insights." Science **340**(6137): 1234168.

Keller, P. J., A. D. Schmidt, A. Santella, K. Khairy, Z. Bao, J. Wittbrodt and E. H. Stelzer (2010). "Fast, high-contrast imaging of animal development with scanned light sheet-based structured-illumination microscopy." Nat Methods **7**(8): 637-642.

Keller, P. J., A. D. Schmidt, J. Wittbrodt and E. H. Stelzer (2008). "Reconstruction of zebrafish early embryonic development by scanned light sheet microscopy." Science **322**(5904): 1065-1069.

Kinoshita, M., K. Murata, K. Naruse and M. Tanaka (2009). Medaka: biology, management, and experimental protocols, John Wiley & Sons.

Kobayashi-Taguchi, K., T. Saitou, Y. Kamei, A. Murakami, K. Nishiyama, R. Aoki, E. Kusakabe, H. Noda, M. Yamashita, R. Kitazawa, T. Imamura and Y. Takada (2022). "Computer-Aided Detection of Quantitative Signatures for Breast Fibroepithelial Tumors Using Label-Free Multi-Photon Imaging." Molecules **27**(10).

Kumar, A., Y. Wu, R. Christensen, P. Chandris, W. Gandler, E. McCreedy, A. Bokinsky, D. A. Colón-Ramos, Z. Bao and M. McAuliffe (2014). "Dual-view plane illumination microscopy for rapid and spatially isotropic imaging." Nature protocols **9**(11): 2555-2573.

McGorty, R., H. Liu, D. Kamiyama, Z. Dong, S. Guo and B. Huang (2015). "Open-top selective plane illumination microscope for conventionally mounted specimens." Optics express **23**(12): 16142-16153.

Migliori, B., M. S. Datta, C. Dupre, M. C. Apak, S. Asano, R. Gao, E. S. Boyden, O. Hermanson, R. Yuste and R. Tomer (2018). "Light sheet theta microscopy for rapid high-resolution imaging of large biological samples." BMC biology **16**: 1-19.

Mizutani, H., S. Ono, T. Ushiku, Y. Kudo, M. Ikemura, N. Kageyama, N. Yamamichi, M. Fujishiro, T. Someya and M. Fukayama (2018). "Transparency‐enhancing technology allows three‐dimensional assessment of gastrointestinal mucosa: a porcine model." Pathology international **68**(2): 102-108.

Orimo, A., P. B. Gupta, D. C. Sgroi, F. Arenzana-Seisdedos, T. Delaunay, R. Naeem, V. J. Carey, A. L. Richardson and R. A. Weinberg (2005). "Stromal fibroblasts present in invasive human breast carcinomas promote tumor growth and angiogenesis through elevated SDF-1/CXCL12 secretion." Cell **121**(3): 335-348.

Planchon, T. A., L. Gao, D. E. Milkie, M. W. Davidson, J. A. Galbraith, C. G. Galbraith and E. Betzig (2011). "Rapid three-dimensional isotropic imaging of living cells using Bessel beam plane illumination." Nat Methods **8**(5): 417-423.

Power, R. M. and J. Huisken (2017). "A guide to light-sheet fluorescence microscopy for multiscale imaging." Nat Methods **14**(4): 360-373.

Prakash, J. and Y. Shaked (2024). "The interplay between extracellular matrix remodeling and cancer therapeutics." Cancer discovery **14**(8): 1375-1388.

Richardson, D. S. and J. W. Lichtman (2015). "Clarifying tissue clearing." Cell **162**(2): 246-257.

Saitou, T. and T. Imamura (2023). "Extended depth of focus two-photon light-sheet microscopy for in vivo fluorescence imaging of large multicellular organisms at cellular resolution." International Journal of Molecular Sciences **24**(12): 10186.

Saitou, T. and T. Imamura (2024). "Enhanced light-sheet illumination by a multi-layered stair-step

phase mask." Japanese Journal of Applied Physics **63**(10): 108002.

Saitou, T., H. Kiyomatsu and T. Imamura (2018). "Quantitative Morphometry for Osteochondral Tissues Using Second Harmonic Generation Microscopy and Image Texture Information." Sci Rep **8**(1): 2826.

Saitou, T., S. Takanezawa, H. Ninomiya, T. Watanabe, S. Yamamoto, Y. Hiasa and T. Imamura (2018). "Tissue Intrinsic Fluorescence Spectra-Based Digital Pathology of Liver Fibrosis by Marker-Controlled Segmentation." Front Med (Lausanne) **5**: 350.

Strnad, P., S. Gunther, J. Reichmann, U. Krzic, B. Balazs, G. De Medeiros, N. Norlin, T. Hiiragi, L. Hufnagel and J. Ellenberg (2016). "Inverted light-sheet microscope for imaging mouse pre-implantation development." Nature methods **13**(2): 139-142.

Susaki, E. A., C. Shimizu, A. Kuno, K. Tainaka, X. Li, K. Nishi, K. Morishima, H. Ono, K. L. Ode and Y. Saeki (2020). "Versatile whole-organ/body staining and imaging based on electrolyte-gel properties of biological tissues." Nature communications **11**(1): 1982.

Susaki, E. A., K. Tainaka, D. Perrin, F. Kishino, T. Tawara, T. M. Watanabe, C. Yokoyama, H. Onoe, M. Eguchi and S. Yamaguchi (2014). "Whole-brain imaging with single-cell resolution using chemical cocktails and computational analysis." Cell **157**(3): 726-739.

Swoger, J., P. Verveer, K. Greger, J. Huisken and E. H. Stelzer (2007). "Multi-view image fusion improves resolution in three-dimensional microscopy." Opt Express **15**(13): 8029-8042.

Takanezawa, S., T. Saitou and T. Imamura (2021). "Wide field light-sheet microscopy with lens-axicon

controlled two-photon Bessel beam illumination." Nat Commun **12**(1): 2979.

Temma, K., R. Oketani, T. Kubo, K. Bando, S. Maeda, K. Sugiura, T. Matsuda, R. Heintzmann, T. Kaminishi and K. Fukuda (2024). "Selective-plane-activation structured illumination microscopy." Nature Methods **21**(5): 889-896.

Tomer, R., L. Ye, B. Hsueh and K. Deisseroth (2014). "Advanced CLARITY for rapid and high-resolution imaging of intact tissues." Nature protocols **9**(7): 1682-1697.

Truong, T. V., W. Supatto, D. S. Koos, J. M. Choi and S. E. Fraser (2011). "Deep and fast live imaging with two-photon scanned light-sheet microscopy." Nat Methods **8**(9): 757-760.

Vettenburg, T., H. I. Dalgarno, J. Nylk, C. Coll-Lladó, D. E. Ferrier, T. Čižmár, F. J. Gunn-Moore and K. Dholakia (2014). "Light-sheet microscopy using an Airy beam." Nat Methods **11**(5): 541-544.

Wakamatsu, Y., S. Pristyazhnyuk, M. Kinoshita, M. Tanaka and K. Ozato (2001). "The see-through medaka: a fish model that is transparent throughout life." Proceedings of the National Academy of Sciences **98**(18): 10046-10050.

Wu, Y., A. Ghitani, R. Christensen, A. Santella, Z. Du, G. Rondeau, Z. Bao, D. Colón-Ramos and H. Shroff (2011). "Inverted selective plane illumination microscopy (i SPIM) enables coupled cell identity lineaging and neurodevelopmental imaging in Caenorhabditis elegans." Proceedings of the National Academy of Sciences **108**(43): 17708-17713.

Wu, Y., P. Wawrzusin, J. Senseney, R. S. Fischer, R. Christensen, A. Santella, A. G. York, P. W. Winter, C. M. Waterman and Z. Bao (2013). "Spatially isotropic four-dimensional imaging with dual-view

plane illumination microscopy." Nature biotechnology **31**(11): 1032-1038.